

1 **Mx1 in hematopoietic cells protects against Thogotovirus infection**

2

3 **Running title: Mx1 in hematopoietic cells restricts Thogotovirus**

4

5 Jan Spitaels<sup>1,2,#</sup>, Lien Van Hoecke<sup>1,2</sup>, Kenny Roose<sup>1,2,3</sup>, Georg Kochs<sup>4,5</sup>, Xavier Saelens<sup>\*1,2,3</sup>

6

7 <sup>1</sup> VIB-UGent Center for Medical Biotechnology, 9052 Ghent, Belgium

8 <sup>2</sup> Department of Biomedical Molecular Biology, Ghent University, 9052 Ghent, Belgium

9 <sup>3</sup> Department of Biochemistry and Microbiology, Ghent University, 9052 Ghent, Belgium

10 <sup>4</sup> Institute of Virology, Medical Center-University of Freiburg, Freiburg, Germany

11 <sup>5</sup> Faculty of Medicine, University of Freiburg, Freiburg, Germany

12

13 \* Contact information for corresponding author: xavier.saelens@vib-ugent.be

14

15 # Current address: eTherNA Immunotherapies N.V., Galileilaan 19, 2845 Niel, Belgium

16

17 Key words: Mx1, bone marrow chimeras, Thogotovirus, myeloid cells

18

19 Abstract word count: 229

20 Text word count: 6117

21

22 **Abstract**

23 *Myxovirus resistance 1 (Mx1)* is an interferon-induced gene that encodes a GTPase that plays an  
24 important role in the defense of mammalian cells against influenza A and other viruses. The Mx1  
25 protein can restrict a number of viruses, independently of the expression of other interferon-induced  
26 genes. *Mx* genes are therefore considered to be an important part of the innate antiviral immune  
27 response. However, the possible impact of *Mx* expression in the hematopoietic cellular compartment  
28 has not been investigated in detail in the course of a viral infection. To address this, we performed  
29 bone marrow chimera experiments using congenic B6.A2G *Mx1*<sup>+/+</sup> and B6.A2G *Mx1*<sup>-/-</sup> mice to study  
30 the effect of *Mx1* expression in cells of hematopoietic versus non-hematopoietic origin. *Mx1*<sup>+/+</sup> mice  
31 were protected and *Mx1*<sup>-/-</sup> mice were susceptible to influenza A virus challenge infection, regardless  
32 of the type of bone marrow cells (*Mx1*<sup>+/+</sup> or *Mx1*<sup>-/-</sup>) the animals had received. Infection with  
33 Thogotovirus, however, revealed that *Mx1*<sup>-/-</sup> mice with a functional *Mx1* gene in the bone marrow  
34 compartment showed reduced liver pathology compared with *Mx1*<sup>-/-</sup> mice that had been grafted with  
35 *Mx1*<sup>-/-</sup> bone marrow. The reduced pathology in these mice was associated with a reduction in  
36 Thogotovirus titers in the spleen, lung and serum. Moreover, *Mx1*<sup>+/+</sup> with *Mx1*<sup>-/-</sup> bone marrow failed  
37 to control Thogotovirus replication in the spleen. *Mx1* in the hematopoietic cellular compartment  
38 thus contributes to protection against Thogotovirus infection.

39 **Importance**

40 Mx proteins are evolutionarily conserved in vertebrates and can restrict a wide range of viruses in a  
41 cell autonomous way. The contribution to antiviral defense of Mx1 expression in hematopoietic cells  
42 remains largely unknown. We show that protection against influenza virus infection requires *Mx1*  
43 expression in the nonhematopoietic cellular compartment. In contrast, *Mx1* in bone marrow-derived  
44 cells is sufficient to control disease and virus replication following infection with a Thogotovirus. This  
45 indicates that next to its well established antiviral activity in nonhematopoietic cells, Mx1 in  
46 hematopoietic cells can also play an important antiviral function. In addition, cells of hematopoietic  
47 origin that lack a functional *Mx1* gene, contribute to Thogotovirus dissemination and associated  
48 disease.

49 **Introduction**

50 Myxovirus resistance proteins are dynamin-like large GTPases that can inhibit a wide array of viruses,  
51 including members of the *Orthomyxoviridae*, *Rhabdoviridae* and *Bunyaviridae* (1). *Mx* genes are  
52 evolutionary conserved in vertebrates and their expression is induced by type I and type III interferon  
53 (2-4). How Mx1 proteins inhibit viral replication is still largely undetermined. It has been shown that  
54 mouse Mx1 can suppress primary transcription of influenza A virus (IAV) genes in the nucleus (5).  
55 Furthermore, we previously reported that murine Mx1 can interact with the polymerase basic 2  
56 (PB2) protein and nucleoprotein (NP) in IAV ribonucleoproteins (vRNPs), and disturb the PB2-NP  
57 interaction (6). Human MxA, the orthologue of mouse Mx1, can also interact with IAV NP (7).  
58 Moreover NP has been shown to be a determinant of the sensitivity of IAVs for Mx1 and MxA (8, 9).  
59 Based on these studies, and on the observation that human MxA – like dynamins – can form ring-like  
60 structures (10-14), we hypothesized that the interaction with IAV PB2 and NP might be mediated by  
61 a ring structure comprised of oligomerized Mx1, which then actively disrupts the PB2-NP interaction  
62 (6). Indirect support for this hypothesis was obtained from the observation that an Mx1 construct  
63 that was only active in the presence of an artificial small compound drug, could disrupt pre-existing  
64 IAV vRNPs (15).

65

66 The GTPase activity of Mx1 and MxA is required for the suppression of IAV replication. Presumably  
67 the GTPase function combined with the 2 hinges that flank the central bundle signaling element that  
68 separates the globular head domain from the extended helical stalk domain, allow Mx proteins to  
69 function as molecular machines that exert a kind of ‘power stroke’. This mechano-chemical transition  
70 might generate latitudinal shear forces between neighboring Mx ring structures that destroy the  
71 functional vRNP structure (16). Next to their antiviral effect against IAV, Mx proteins can also restrict  
72 Thogoto virus (THOV, a member of the *Orthomyxoviridae* family) replication. Mouse Mx1, which is  
73 only active in the cell nucleus, inhibits THOV multiplication (17). It has also been shown that human  
74 MxA can interact with the NP molecules of the THOV vRNPs. This interaction prevents THOV vRNPs  
75 from entering the nucleus (18, 19).

76

77 The *Orthomyxoviridae* family currently comprises seven genera: *Influenza A*, *B*, *C* and *D*,  
78 *Thogotovirus*, *Quarantavirus* and *Isavirus* (20-22). Influenza A and B viruses are important human  
79 respiratory pathogens. THOV is a tick-borne virus that has small rodents as natural hosts and very  
80 rarely causes zoonotic infection (23, 24). When people become infected with IAV, the first cells that  
81 are targeted, are the airway epithelial cells. After binding, endocytosis and membrane fusion, the  
82 viral vRNPs are released into the cytoplasm. These then enter the nucleus, where transcription and

83 replication will take place (reviewed in (25)). The incoming vRNPs first direct the synthesis of viral  
84 mRNA (primary transcription), which is transported to the cytosol and translated. Newly produced  
85 PB1, PB2, Polymerase acidic (PA) and NP migrate to the nucleus to start initiate replication of the  
86 viral genome and boost transcription. The resulting progeny viral RNA molecules form vRNPs, and  
87 leave the nucleus, ready for packaging and budding (26). Although THOV has not been studied as  
88 elaborately as IAV, it has been shown that both viruses are structurally and genetically similar (27-  
89 33). Several studies have also pointed out that their replication cycles are comparable (17-19, 34-40).  
90 When a mouse becomes infected with THOV, the virus replicates and spreads rapidly to different  
91 sites in the mouse body to eventually kill the mouse (41). A similar pathogenesis in mice following  
92 infection with the related Dhori virus has been reported: the virus could be detected in multiple  
93 organs such as the brain, lungs, thymus, spleen, adrenal glands, and liver (42). However, the main  
94 target organ of THOV and Dhori virus is the liver, where these viruses can replicate to very high titers  
95 and cause severe coagulative zonal necrosis leading to the rapid death of the infected mouse (17,  
96 42).

97

98 Mx proteins exert their antiviral activity in a cell autonomous way. Haller and coworkers reported  
99 that athymic (nude) mice, which carry a functional *Mx1* gene, survived intracerebral infection with a  
100 neurotropic IAV strain, demonstrating that *Mx1*-positive mice do not require a functional T cell  
101 system to survive the infection (43). Later, the same lab reported that *in vivo* resistance to a  
102 pneumotropic, neurotropic or hepatotropic strain of IAV was largely independent of whether  
103 macrophages carried a functional *Mx1* gene or not (44). These studies showed that *Mx1* expression  
104 in hematopoietic cells does not play a major role in the resistance against IAV infection. It is also  
105 important to note that almost all mouse genetic studies on the contribution of interferon-induced  
106 gene products to antiviral defense in the immune cell compartment have been carried out in  
107 laboratory mouse strains that lack a functional *Mx1* gene (45).

108

109 The aim of the present study is to examine the role of *Mx1* expression in immune cells for the  
110 antiviral host defense. We show that in bone marrow chimeric mice the protection by *Mx1* against  
111 IAV infection depends solely on the genotype of the stromal (nonhematopoietic) cells as previously  
112 demonstrated by Haller *et al.* (43). In striking contrast, challenge infection with THOV showed that  
113 *Mx1* expression in bone marrow-derived cells is sufficient to markedly reduce virus replication and  
114 dissemination, and delay morbidity in mice.

115 **Materials and methods**

116 **Ethics statement.** All animal experiments described in this study were conducted according to the  
117 national (Belgian Law 14/08/1986 and 22/12/2003, Belgian Royal Decree 06/04/2010) and European  
118 legislation (EU Directives 2010/63/EU, 86/609/EEC). All experiments on mice and animal protocols  
119 were approved by the ethics committee of Ghent University (permit numbers LA1400091 and  
120 EC2015-027).

121

122 **Mice.** Mice were bred in-house under Specific Pathogen Free (SPF) conditions. Mice were housed in  
123 individually ventilated cages, in a temperature-controlled environment with 12h light/dark cycles,  
124 with food and water *ad libitum*. Congenic B6.A2G-*Mx1* (*Mx1*<sup>+/+</sup>) mice with a functional A2G *Mx1*  
125 allele were kindly provided by Peter Stäheli (University of Freiburg, Germany). Congenic B6.A2G-*Mx1*  
126 (*Mx1*<sup>-/-</sup>) carrying the defective C57BL/6J *Mx1* allele were generated in our laboratory by crossing  
127 B6.A2G-*Mx1* (*Mx1*<sup>+/+</sup>) with C57BL/6J (*Mx1*<sup>-/-</sup>) mice, and subsequent crossing of the heterozygous  
128 offspring. Mouse genomic DNA was isolated from tail biopsies following digestion at 55°C in buffer  
129 containing 50 mM Tris-HCl (pH8.0), 10 mM EDTA, 100 mM NaCl, 0.1% SDS and 1 mg/ml proteinase K.  
130 A PCR was performed using the following primers: 5'-GGAGCTCACCTCCACATCT-3', 5'-  
131 AGCATGGCTGTGTACAAGCA-3', and 5'-CGAAGGCAGTTTGGACCATCT-3'. PCR consisted of a 1 min  
132 denaturation step at 94°C, a 1 min annealing step at 61°C, and a 1 min polymerization step at 72 °C  
133 for 1min (40 cycles). The resulting PCR products were visualized by agarose gel electrophoresis.

134

135 **Bone marrow chimera mice.** Starting one week before and until three weeks after irradiation, mice  
136 were given water containing 0.2% neomycin *ad libitum*. Mice were subjected to lethal total body  
137 irradiation (10 Grey) with an X-Rad 320 Biological Irradiator (Precision X-Ray (PXi), North Brandford,  
138 Connecticut, USA), and 24h later they were reconstituted with syngeneic or allogeneic bone marrow  
139 cells (8-10 x 10<sup>6</sup>) that were harvested from femurs of age-matched mice. Experimental transfers were  
140 as follows: B6.A2G *Mx1*<sup>-/-</sup> donors into B6.A2G *Mx1*<sup>-/-</sup> recipients (*Mx1*<sup>-/-</sup> → *Mx1*<sup>-/-</sup>), B6.A2G *Mx1*<sup>-/-</sup>  
141 donors into B6.A2G *Mx1*<sup>+/+</sup> recipients (*Mx1*<sup>-/-</sup> → *Mx1*<sup>+/+</sup>), B6.A2G *Mx1*<sup>+/+</sup> donors into B6.A2G *Mx1*<sup>+/+</sup>  
142 recipients (*Mx1*<sup>+/+</sup> → *Mx1*<sup>+/+</sup>), and B6.A2G *Mx1*<sup>+/+</sup> donors into B6.A2G *Mx1*<sup>-/-</sup> recipients (*Mx1*<sup>+/+</sup> →  
143 *Mx1*<sup>-/-</sup>). Animals were allowed to recover and reconstitute their hematopoietic cellular compartment  
144 for eight weeks. Only healthy mice without obvious signs of graft-versus-host disease were used in  
145 experiments.

146

147 **Virus challenge.** Mice were challenged with 10 lethal dose 50% (LD<sub>50</sub>) (approximately 170 PFU) of  
148 mouse adapted (ma) influenza A/Puerto Rico/8/34 (PR8) (H1N1) or with 10<sup>3</sup> PFU of THOV SiAr 126

149 (17). The challenge dose was administered intranasally in a volume of 50  $\mu$ l (maPR8) or  
150 intraperitoneally in a volume of 100  $\mu$ l (THOV) to mice that were anesthetized with a mixture of  
151 ketamine (10 mg/kg) and xylazine (60 mg/kg). Morbidity was monitored during six (maPR8) or four  
152 (THOV) days post infection. Mice that had lost 25% or more of their bodyweight were euthanized by  
153 cervical dislocation.

154

155 **Determination of influenza lung virus titers.** Mice were sacrificed at different time points after  
156 infection by intraperitoneal injection of pentobarbital (125  $\mu$ g/g). The mouse lungs were removed  
157 aseptically, and the left lobe was snap-frozen in liquid nitrogen. Lung extracts were prepared by  
158 homogenizing the lungs in PBS using metal beads. Cell debris was cleared by centrifugation for 10  
159 min at 400g and 4°C. Cleared lung extracts were stored at -80°C. Influenza virus titers were  
160 determined in triplicate by titration on MDCK cells. Briefly, MDCK monolayers were infected for 1h  
161 with 500  $\mu$ l of serial 1:10 dilutions of the lung homogenates in a 12-well plate in serum-free DMEM  
162 medium supplemented with penicillin and streptomycin. Following inoculation, the supernatant was  
163 replaced by medium containing 2  $\mu$ g/ml trypsin and 0.6% avicel RC-851 (FMC Biopolymers). Two days  
164 after infection, the cells were fixed with 4% paraformaldehyde, and permeabilized with PBS  
165 containing 0.2% Triton X-100. Plaques were stained using a mouse monoclonal antibody against the  
166 ectodomain of the influenza M2 protein, and an HRP-conjugated anti-mouse IgG antibody (Sheep  
167 anti-mouse IgG HRP, GE Healthcare, UK). Plaques were then visualized by using TrueBlue peroxidase  
168 substrate (Seracare, Gaithersburg, MD, USA).

169

170 **Determination of Thogoto liver virus titers.** Mice were killed by cervical dislocation, the liver was  
171 removed aseptically, and one of the lobes was used for histochemistry. Liver extracts were made by  
172 homogenizing the livers in PBS using metal beads. Cell debris was cleared by centrifugation for 10  
173 min at 400g and 4°C. Cleared liver extracts were stored at -80°C before use. THOV titers were  
174 determined in triplicate by titration on Vero cells. Monolayers of Vero cells were infected for 1h with  
175 1 ml of serial 1:10 dilutions of the liver homogenates in a 6-well plate in DMEM medium  
176 supplemented with 2% fetal calf serum and 20 mM HEPES pH 7.3. Following inoculation, the  
177 supernatant was replaced by medium containing 0.6% avicel RC-951 (FMC Biopolymers). Four days  
178 after infection, the cells were fixed with 4% paraformaldehyde. The cell monolayers were stained  
179 with a crystal violet solution (1% crystal violet + 1% methanol + 20% ethanol) for approximately 15  
180 minutes at room temperature. The crystal violet solution was then removed and the wells were  
181 washed with water to reveal the plaques.

182

183 **Histopathological examination of livers.** Livers of bone marrow chimeric mice were excised at 0, 2 or  
184 4 dpi. After fixation in 4% paraformaldehyde (PFA) and embedding in paraffin, livers were sectioned  
185 at 5  $\mu$ m. Sections were used for haematoxylin/eosin staining and immunohistochemical analysis.  
186 After incubation with primary and secondary biotin-conjugated antibodies immunoreactivity was  
187 revealed using the ABC-HRP Kit (Vector Laboratories, Burlingame, California USA) and the sections  
188 were counterstained with hematoxylin. Images were obtained with an Axioscan.Z1 slide scanner  
189 (Zeiss, Oberkochen, Germany), and were analyzed with ZEN Lite software (Zeiss, Oberkochen,  
190 Germany).

191

192 **ALT/AST assay.** Blood was taken by retro-orbital bleeding after sedation of the mice with  
193 pentobarbital (125  $\mu$ g/g). To prepare mouse serum, the blood samples were allowed to clot  
194 overnight at 4°C. The next day the clot was removed and samples were centrifuged at 14000 rpm for  
195 3 minutes. Serum samples were stored at -20°C before use. Levels of aspartate aminotransferase  
196 (AST) and alanine aminotransferase (ALT) were measured using a Hitachi kit and apparatus in the  
197 Clinical Biology Laboratory of Ghent University Hospital.

198

199 **Real-time quantitative PCR (RT-qPCR).** Mice of each group were sacrificed just prior to and on day 3  
200 and 6 after IAV infection by intraperitoneal injection of pentobarbital (125  $\mu$ g/g). The mouse lungs  
201 were removed aseptically, and the left lobe was snap-frozen in liquid nitrogen. Lung extracts were  
202 made by homogenizing the lungs in PBS using metal beads. Cell debris was cleared by centrifugation  
203 for 10 min at 400g and 4°C. Cleared lung extracts were stored at -80°C until use. RNA was isolated  
204 with the High Pure RNA Isolation Kit (11828665001, Roche) as indicated by the manufacturer. Total  
205 mRNA was converted to cDNA by RT-PCR using oligo-dT reaction (Transcriptor First Strand cDNA  
206 Synthesis Kit, 04897030001, Roche). Ten nanogram of cDNA was used for each quantitative PCR  
207 (qPCR) reaction, and triplicate reactions were setup in 384-well plates. qPCR reactions based on SYBR  
208 green detection, were performed using a LightCycler (Roche). qPCR-data were analyzed using the  
209 qbase+ software packet (Biogazelle, Zwijnaarde, Belgium).

210 The primers used in this study are as follows. M1/2 forward: 5'-GGGAAGAACACCGATCTTGA-3'; M1/2  
211 reverse: 5'-CGGTGAGCGTGAACACAAAT-3'; NA forward: 5'-CATCTCTTTGTCCCATCCGT-3'; NA reverse:  
212 5'-GTCCTGCATTCCAAGTGAGA-3'; HA forward: 5'-GAGGAGCTGAGGGAGCAAT-3'; HA reverse: 5'-  
213 GCCGTTACTCCGTTTGTGTT-3'; PB1 forward: 5'-CCTCCTTACAGCCATGGGA-3'; PB1 reverse: 5'-  
214 GTGCTCCAGTTTCGGTGTGTT-3'; PB2 forward: 5'-GGATCAGACCGAGTGATGGT-3'; PB2 reverse: 5'-  
215 CCATGCTTTAGCCTTTCGACT-3'; PA forward: 5'-CATCAATGAGCAAGGCGAGT-3'; PA reverse: 5'-  
216 GCCCTGTAGTGTGCAAAT-3'; NP forward: 5'-CAGCCTAATCAGACCAAATG-3'; NP reverse: 5'-  
217 TACCTGCTTCTCAGTTCAAG-3'; NS1 forward: 5'-TTCACCATTGCCTTCTCTTC-3'; NS1 reverse: 5'-



218 CCCATTCTCATTACTGCTTC-3'; HPRT1 forward: 5'-AGTGTGGATACAGGCCAGAC-3'; HPRT1 reverse: 5'-  
219 CGTGATTCAAATCCCTGAAGT-3'; UBC forward: 5'-AGGTCAAACAGGAAGACAGACGTA-3'; UBC reverse:  
220 5'-TCACACCCAAGAACAAGCACA-3'; GAPDH forward: 5'-TGAAGCAGGCATCTGAGGG-3'; GAPDH  
221 reverse: 5'-CGAAGGTGGAAGAGTGGGAG-3'; TBP forward: 5'-TCTACCGTAATCTTGGCTGTAAA-3'; TBP  
222 reverse: 5'-TTCTCATGATGACTGCAGCAAA-3'; RPL13A forward: 5'-CCTGCTGCTCTCAAGTT-3'; RPL13A  
223 reverse: 5'-TGGTTGCTACTGCCTGGTACTT-3'; actin forward: 5'-GCTTCTAGGCGGACTGTTACTGA-3';  
224 actin reverse: 5'-GCCATGCCAATGTTGTCTCTTAT-3'.

225

226 **Antibodies.** A polyclonal antiserum against mouse Mx1 was generated by immunizing New Zealand  
227 White rabbits with a synthetic, high-performance liquid chromatography-purified peptide  
228 CKKFLKRRLLRLDEARQKLAKFSD (C terminus of the Mx1 protein) and purified as described (6). M2e-  
229 specific monoclonal antibody was produced in our laboratory. Briefly, hybridomas that produce M2e-  
230 specific monoclonal antibodies were isolated as described (46). After subcloning, these hybridoma  
231 cultures were scaled up and monoclonal antibodies were purified from the culture supernatant with  
232 a protein A column (GE Healthcare). Polyclonal anti-Thogoto virus NP antibody, (antiserum, rabbit),  
233 was generated in the laboratory of Georg Kochs (University of Freiburg, Germany) (32). Polyclonal  
234 anti-CD45 antibody (rabbit) was obtained from Abcam (ab10558). Biotinylated anti-rabbit antibody  
235 (goat) was obtained from Vector Laboratories (BA-1000).

236

237 **Statistical analysis.** The obtained data were analyzed using Graphpad Prism 7 or Genstat software.  
238 Methods used in Genstat are described below. Statistical tests were performed in Graphpad Prism 7  
239 software and are mentioned in the figure legends. Relative bodyweight data were analyzed as  
240 repeated measurements using the residual maximum likelihood (REML) approach as implemented in  
241 Genstat v19 (47). Briefly, a linear mixed model with replicate, genotype, time and genotype x time  
242 interaction as fixed terms, and subject time used as residual term, was fitted to the data. Times of  
243 measurement were set at equal intervals and an autoregressive correlation structure of order 1 with  
244 equal variances (*i.e.* homogeneity across time) was selected as best model fit in all cases, based on  
245 the Aikake Information Coefficient. Significances of the fixed terms and significances of changes in  
246 differences between genotype effects over time were assessed by an F-test. Viral titers were  
247 analyzed with a Hierarchical Generalized Linear Mixed Model (HGLMM; fixed model: poisson  
248 distribution, log link; random model: gamma distribution, log link) as implemented in Genstat v19  
249 (47). Titers below the detection limit have been imputed with values generated as a random sample  
250 from a skewed left tailed beta distribution Beta (5,1). Fixed terms include GENOTYPE, DPI, TISSUE and  
251 their two-way and three-way interaction, while REPLICATE was set as random term. T- statistics were  
252 used to assess the significance of tissue-specific genotype effects at dpi = 2 and 4 (on the

253 transformed scale). Estimated mean values were obtained as predictions from the HGLMM, formed  
254 on the scale of the response variable. RT-qPCR data were compared with a Generalized Linear Mixed  
255 Model (GLMM) (fixed model: Poisson distribution, log link; random model: gamma distribution, log  
256 link) as implemented in Genstat v19 (47) fitted to RT-qPCR expression data of PB1, PB2, PA, NP, HA,  
257 NA, M and NS genes simultaneously. The linear predictor vector of the values can be written as  
258 follows:  $\log(\mu) = \eta = X\beta + Zv$ , where the matrix X is the design matrix for the fixed terms genotype,  
259 time and genotype x time,  $\beta$  is their vector of regression coefficients, Z is the design matrix for the  
260 random term (i.e. gene, replicate and gene x replicate), and v is the corresponding vector of random  
261 effect having a gamma distribution. The significance of the fixed interaction term genotype x time  
262 was assessed by a Wald test. Significance of the regression coefficients were assessed by a t-test.  
263 Estimated mean values and their standard errors were obtained as predictions from the GLMM,  
264 formed on the scale of the response variable. A Hierarchical Generalized Linear Mixed Model  
265 (HGLMM; fixed model: Poisson distribution, log link; random model: gamma distribution, log link) as  
266 implemented in Genstat v19 (47) has been fitted to the "ALT" and "AST" data. Fixed terms include  
267 GENOTYPE, DPI and their interaction, while REPLICATE was set as random term. T statistics were  
268 used to assess the significance of time-specific genotype effects (on the transformed scale).  
269 Estimated mean values were obtained as predictions from the HGLMM, formed on the scale of the  
270 response variable.

271 **Results**272 **Resistance to influenza A virus infection primarily depends on the *Mx1* genotype of the recipient**

273 Most immune cells originate from multipotent hematopoietic stem cells in the bone marrow. To  
274 address the possible role of *Mx1* as a virus restriction factor in this compartment, we generated all  
275 four possible bone marrow chimeric mice between B6.A2G *Mx1*<sup>-/-</sup> and B6.A2G *Mx1*<sup>+/+</sup> mice (Fig 1A).  
276 Eight weeks after bone marrow transfer, the chimeric mice were infected with 10 LD<sub>50</sub> of maPR8  
277 virus, and bodyweight was monitored during 6 days post infection (dpi). B6.A2G *Mx1*<sup>-/-</sup> recipient mice  
278 displayed significantly more bodyweight loss than B6.A2G *Mx1*<sup>+/+</sup> recipient mice regardless of the  
279 donor genotype (Fig 1B). In addition, infection with maPR8 virus of mice with a functional *Mx1* gene  
280 in the stromal cells did not result in bodyweight loss regardless of the donor genotype (Fig 1B). Lung  
281 virus loads were significantly lower in the B6.A2G *Mx1*<sup>+/+</sup> recipients than in B6.A2G *Mx1*<sup>-/-</sup> recipients  
282 on day 3 and 6 after infection. We observed no significant difference in viral loads between *Mx1*<sup>-/-</sup>  
283 mice that had been reconstituted with bone marrow from either donor and neither between the  
284 *Mx1*<sup>+/+</sup> recipients that were reconstituted with *Mx1*<sup>-/-</sup> or *Mx1*<sup>+/+</sup> donor bone marrow (Fig 1C). It has  
285 been reported that in cells that stably express *Mx1*, primary transcription of IAV genes is reduced and  
286 this reduction is more pronounced for the larger genes encoding the polymerase subunits compared  
287 with the shorter viral transcripts (5). To ascertain that such a differential effect might also be  
288 observed *in vivo*, we quantified the individual viral mRNA levels in the mouse lung on day 3 and 6  
289 after infection by RT-qPCR. Three and six days after infection, the viral mRNA levels were much lower  
290 in the lungs of B6.A2G *Mx1*<sup>+/+</sup> compared to those in lungs of B6.A2G *Mx1*<sup>-/-</sup> recipient mice (Fig 1D). In  
291 contrast to what was previously reported by Pavlovic *et al.* (5), we noticed that the inhibiting effect  
292 of *Mx1* was equally strong for the shorter and longer viral RNA segments (Fig 1E). Together, these  
293 data show that the *Mx1* genotype of the recipient rather than the donor determines the outcome of  
294 maPR8 virus infection, both in terms of controlling disease and viral replication.

295

296 ***Mx1* in hematopoietic cells contributes to the control of Thogotovirus infection**

297 We next addressed the possible contribution of *Mx1* in the stromal versus hematopoietic cells for  
298 control of THOV infection. The rationale for choosing this virus is threefold: (i) THOV, like IAV, is a  
299 member of the *Orthomyxoviridae*, (ii) the virus is also sensitive to murine *Mx1* (17), and (iii) small  
300 rodents are natural hosts of this virus (24). Bone marrow chimeric mice were infected  
301 intraperitoneally with 1000 plaque forming units (PFU) of THOV (Sicilian SiAr 126 isolate), and  
302 bodyweight and morbidity were monitored daily during four days after infection. *Mx1*<sup>+/+</sup> mice that  
303 received *Mx1*<sup>+/+</sup> bone marrow showed no signs of morbidity or bodyweight loss, and *Mx1*<sup>-/-</sup> recipients  
304 that had been reconstituted with *Mx1*<sup>-/-</sup> bone marrow lost significantly more bodyweight than all

305 other chimeric groups and became moribund by day 4 post infection (Fig 2A). Interestingly, B6.A2G  
306 *Mx1<sup>+/+</sup>* mice that had received *Mx1<sup>-/-</sup>* bone marrow lost significantly more bodyweight than B6.A2G  
307 *Mx1<sup>-/-</sup>* mice that had received *Mx1<sup>+/+</sup>* bone marrow, indicating a protective role for *Mx1* expression in  
308 hematopoietic cells in this infection model. Surprisingly, liver viral titers did not reflect these findings.  
309 The THOV titers in the liver of the B6.A2G *Mx1<sup>-/-</sup>* recipient mice were very high (approximately 10<sup>6</sup> to  
310 10<sup>7</sup> PFU/g; the two fold lower virus load in the *Mx1<sup>+/+</sup>* recipients did not reach statistical significance)  
311 (Fig 2B). In contrast, THOV virus could not be detected in liver extracts from infected B6.A2G *Mx1<sup>+/+</sup>*  
312 recipient mice on 4 dpi independent of the donor genotype (Fig 2B). These data suggest that *Mx1*  
313 expression in hematopoietic cells contributes to the control of THOV-associated morbidity and, to a  
314 limited extent, viral replication in the liver of B6.A2G *Mx1<sup>-/-</sup>* recipient mice.

315

#### 316 ***Mx1<sup>+/+</sup>* expression in hematopoietic cells reduces THOV-associated liver pathology in B6.A2G *Mx1<sup>-/-</sup>*** 317 **recipients**

318 THOV infection was previously shown to cause severe liver pathology in *Mx1<sup>-/-</sup>* mice, but not in  
319 *Mx1<sup>+/+</sup>* mice (17). To examine the possible contribution of donor-derived *Mx1* on THOV-associated  
320 liver damage, we performed histological analysis on the bone marrow chimeric mice sacrificed on  
321 day 4 after THOV infection. Livers isolated from *Mx1<sup>-/-</sup>* mice that had been reconstituted with *Mx1<sup>-/-</sup>*  
322 bone marrow appeared very pale and friable in comparison to the livers from mice in the three other  
323 groups, which had a normal brown-red color and firm tissue. Liver sections were prepared, stained  
324 with hematoxylin and eosin (H&E) and analyzed microscopically. H&E-stained liver tissue from THOV  
325 infected *Mx1<sup>-/-</sup>* mice reconstituted with *Mx1<sup>-/-</sup>* bone marrow showed lesions with focal to widespread  
326 liver cell necrosis (Fig 2C). Interestingly, liver tissue from *Mx1<sup>+/+</sup>* recipient mice reconstituted with  
327 *Mx1<sup>-/-</sup>* bone marrow also showed lesions, although these lesions appeared to be in an earlier stage of  
328 necrosis compared to those in mice that are *Mx1<sup>-/-</sup>* in both the stromal and immune cell  
329 compartment. This is manifested as foci in the liver tissue where structure and cell architecture are  
330 lost, but cell nuclei are still observed. B6.A2G *Mx1<sup>+/+</sup>* recipient's liver tissue appeared normal and  
331 showed no lesions, irrespective of the donor genotype (Fig 2C). In summary, these results show that  
332 *Mx1* in cells with a hematopoietic origin can reduce or at least delay liver pathology associated with  
333 THOV infection in B6.A2G *Mx1<sup>-/-</sup>* recipient mice.

334

335 To quantify the degree of liver damage resulting from the THOV infection, alanine aminotransferase  
336 (ALT) and aspartate aminotransferase (AST) levels were determined in serum of the bone marrow  
337 chimeric mice at 4 dpi. The serum levels of both ALT and AST were markedly increased in THOV-  
338 infected *Mx1<sup>-/-</sup>* mice reconstituted with *Mx1<sup>-/-</sup>* bone marrow compared with the two *Mx1<sup>+/+</sup>* recipient  
339 groups (Fig 2D and 2E). Interestingly, THOV infection of irradiated *Mx1<sup>-/-</sup>* mice reconstituted with

340 *Mx1*<sup>+/+</sup> bone marrow was associated with intermediate levels of both enzymes. This is in accordance  
341 with the histological scoring of the liver sections, further substantiating that *Mx1*<sup>+/+</sup> hematopoietic  
342 cells can contribute to protection against THOV infection in mice that lack *Mx1* in the stromal  
343 compartment.

344

#### 345 **Delayed THOV-associated morbidity in *Mx1*<sup>-/-</sup> mice grafted with *Mx1*<sup>+/+</sup> bone marrow**

346 The previous results led to the hypothesis that *Mx1* expression in the hematopoietic compartment  
347 can delay the course of the THOV infection-associated pathology in *Mx1*<sup>-/-</sup> recipient mice. Therefore,  
348 we performed additional THOV experiments in the chimeric mice to compare virus replication and  
349 pathology at day 2 and 4 after infection. Before infection, all mice had healthy liver tissue (Fig 3A).  
350 Two days after infection *Mx1*<sup>-/-</sup> recipient mice already showed clear zones of cellular influx (Fig 3A).  
351 These zones were markedly larger and more numerous in the *Mx1*<sup>-/-</sup> mice reconstituted with *Mx1*<sup>-/-</sup>  
352 bone marrow than in the *Mx1*<sup>+/+</sup> mice reconstituted with *Mx1*<sup>-/-</sup> donor cells. Amongst the *Mx1*<sup>+/+</sup>  
353 recipient mice that had received *Mx1*<sup>-/-</sup> bone marrow, a few small zones of cellular influx were  
354 observed after 2 days of infection. Four days after infection, *Mx1*<sup>+/+</sup> recipient mice showed no zones  
355 of cellular influx or liver cell necrosis. In contrast, all *Mx1*<sup>-/-</sup> recipients showed clear zones of cellular  
356 influx and/or liver cell necrosis. Livers from mice that lack *Mx1* in both the stromal and immune cell  
357 compartment showed clear zones of liver cell necrosis and only a few small zones of cellular influx.  
358 Interestingly, livers from *Mx1*<sup>-/-</sup> mice that had received *Mx1*<sup>+/+</sup> donor cells, showed large zones of  
359 cellular influx. In the largest influx zones a center of necrotic cells could be observed (Fig 3A, arrows).  
360 This indicates that the THOV infection-related pathology is at an earlier state in *Mx1*<sup>-/-</sup> mice that  
361 received *Mx1*<sup>+/+</sup> bone marrow than in *Mx1*<sup>-/-</sup> mice that received *Mx1*<sup>-/-</sup> bone marrow.

362

363 Four days after THOV infection it was clear that *Mx1*<sup>-/-</sup> mice that received *Mx1*<sup>-/-</sup> bone marrow show  
364 the highest ALT and AST levels with an average of approximately 4000 and 10 000 U/L, respectively.  
365 *Mx1*<sup>+/+</sup> recipients showed only background levels of ALT and AST. In *Mx1*<sup>-/-</sup> mice reconstituted with  
366 *Mx1*<sup>+/+</sup> bone marrow, intermediate ALT and AST levels were detected in the serum (approximately  
367 100 and 500 U/L, respectively) (Fig 3B and 3C). The differences between the ALT and AST levels  
368 between the four groups are most pronounced at 4 dpi. At two dpi the ALT and AST levels of the  
369 *Mx1*<sup>-/-</sup> mice that received *Mx1*<sup>-/-</sup> bone marrow are comparable to the AST and ALT levels of the *Mx1*<sup>-/-</sup>  
370 mice reconstituted with *Mx1*<sup>+/+</sup> bone marrow at four dpi. This shows that the presence of a functional  
371 *Mx1* gene in hematopoietic cells can delay the THOV infection-related liver pathology in mice.

372

373 We also assessed the presence of THOV in the spleen, lung and serum next to the liver. Similar to the  
374 experiment shown in Figure 2, liver viral titers at 4 dpi were highest in the *Mx1*<sup>-/-</sup> mice that received

375 *Mx1*<sup>-/-</sup> bone marrow, 1.5 to 2 logs lower in *Mx1*<sup>-/-</sup> mice that received *Mx1*<sup>+/+</sup> bone marrow, and were  
376 undetectable in both *Mx1*<sup>+/+</sup> recipient groups (Fig 4A). At 2 dpi, liver viral titers in both *Mx1*<sup>-/-</sup>  
377 recipient groups are lower compared to the viral titers at 4 dpi. *Mx1*<sup>+/+</sup> recipient mice had  
378 undetectable liver viral titers at 2 dpi. THOV was detectable in lung and serum sampled from *Mx1*<sup>-/-</sup>  
379 mice that received *Mx1*<sup>-/-</sup> bone marrow but in none of the other groups (Fig 4B and C). Strikingly, the  
380 spleen viral titers show a remarkable difference compared to the titers in the liver, lung and serum.  
381 Spleen THOV titers were highest in the *Mx1*<sup>-/-</sup> mice that received *Mx1*<sup>-/-</sup> bone marrow group at 2 and  
382 4 dpi (Fig 4D). However, spleen viral titers are below the detection limit in *Mx1*<sup>-/-</sup> mice that received  
383 *Mx1*<sup>+/+</sup> bone marrow. Surprisingly, *Mx1*<sup>+/+</sup> mice that received *Mx1*<sup>-/-</sup> bone marrow show viral titers  
384 that are only 4 fold lower than *Mx1*<sup>-/-</sup> mice that received *Mx1*<sup>+/+</sup> bone marrow at 2 dpi and 9 fold  
385 lower at 4 dpi. Thus a functional *Mx1* gene in the hematopoietic cellular compartment is sufficient to  
386 control THOV spread to the lungs, spleen and serum.

387

#### 388 ***Mx1* expression negatively correlates with THOV NP expression in stromal and bone marrow-** 389 **derived cells**

390 The above data show that dissemination of THOV infection depends on the *Mx1* genotype of the  
391 hematopoietic and/or stromal compartment. To demonstrate the cellular import of THOV infection,  
392 liver tissue slides of bone marrow chimeras were stained with antibodies specific for CD45 (myeloid  
393 cell marker), mouse *Mx1*, or THOV NP two and four dpi. Accumulation of myeloid cells could be  
394 detected in all chimeric groups except in *Mx1*<sup>+/+</sup> mice that received *Mx1*<sup>+/+</sup> bone marrow (Fig 5). In  
395 livers of *Mx1*<sup>-/-</sup> mice that received *Mx1*<sup>-/-</sup> bone marrow none of the cells stained positive for *Mx1*.  
396 Surprisingly, the only cells that stained positive for THOV NP – these cells are productively infected by  
397 THOV – are cells in the zones of cellular infiltrates. By contrast, cells in the cellular infiltrate zones in  
398 livers of *Mx1*<sup>-/-</sup> mice that received *Mx1*<sup>+/+</sup> bone marrow stained positive for CD45 and *Mx1*, but not  
399 for THOV NP. In liver tissue of *Mx1*<sup>+/+</sup> mice that received *Mx1*<sup>-/-</sup> bone marrow the opposite was  
400 observed. Here, the cells in the cellular infiltrate zone stained positive for CD45 and THOV NP, but  
401 not for *Mx1*. As expected, there are no zones of cellular infiltration in livers of *Mx1*<sup>+/+</sup> mice that  
402 received *Mx1*<sup>+/+</sup> bone marrow, and liver cells only stained positive for mouse *Mx1*. Four days after  
403 infection, liver tissue of *Mx1*<sup>-/-</sup> mice that received *Mx1*<sup>-/-</sup> bone marrow displayed ample liver cell  
404 necrosis (Figure 5). This loss of structure in the liver tissue also influenced the background staining.  
405 Except for the large zones of cell infiltration in liver tissue of *Mx1*<sup>-/-</sup> mice that received *Mx1*<sup>+/+</sup> bone  
406 marrow, staining for CD45, mouse *Mx1* and THOV NP at 4 dpi was comparable with that at 2 dpi.  
407 Together, these data suggest that cells that make up the zones of cellular infiltration are CD45<sup>+</sup>, that  
408 these CD45<sup>+</sup> cells first encounter THOV then infiltrate the peripheral organs and thus disseminate the  
409 infection.

410 **Discussion**

411 In mice, it is well established that expression of a functional Mx1 protein can protect against a  
412 challenge dose of IAV or THOV that otherwise causes severe morbidity and mortality in mice without  
413 a functional *Mx1* gene. However, whether *Mx1* expression is induced in every IFN-responsive cell  
414 upon infection, and whether *Mx1* is needed for their proper functioning, remains an open question.  
415 Several studies have shown the importance of an IFN response in cell types involved in the adaptive  
416 immune response after IAV infection (48-50). These studies make it tempting to hypothesize that  
417 Mx1 can also play a role in the protection against viral infection of cell types that are involved in  
418 adaptive immunity. Here, we generated *Mx1* bone marrow chimeras, allowing us to investigate the  
419 possible effect of *Mx1* when it is primarily expressed by bone marrow-derived cells or stromal cells.  
420 However, some bone marrow-derived cell types, such as Langerhans cells (51) and mesenchymal  
421 stromal cells (reviewed in (52)), are resistant to lethal total body irradiation. Consequently, these cell  
422 types will have the genotype of the bone marrow recipient.

423

424 Because of the dominant effect of the presence or lack of *Mx1* expression in epithelial cells, the data  
425 obtained in this IAV infection model do not answer the question if *Mx1* can play a role in bone  
426 marrow-derived immune cells. Conceivably, the maPR8 virus infection model, characterized by a  
427 preferred tropism for epithelial cells, is not the best suited for answering the question. It was  
428 recently reported that internal genes of highly pathogenic H5N1 viruses can facilitate replication in  
429 myeloid cells and lead to severe disease in *Mx1*-deficient mice (53). It is therefore possible that  
430 challenge infections of *Mx1* bone marrow chimeras with such influenza viruses could have revealed a  
431 more pronounced effect on the infection outcome in animals that received *Mx1*<sup>+/+</sup> bone marrow.

432

433 Instead of exploring the outcome of infections with a highly pathogenic influenza virus, we turned to  
434 THOV challenge infections. Bone marrow chimeras were infected intraperitoneally with a high dose  
435 of THOV. Morbidity was somewhat different from that seen in the IAV infection model, in that *Mx1*<sup>-/-</sup>  
436 mice that received *Mx1*<sup>+/+</sup> bone marrow showed less body weight loss than *Mx1*<sup>+/+</sup> mice that received  
437 *Mx1*<sup>-/-</sup> bone marrow. Remarkably, liver viral titers at 4 dpi were very high for all the *Mx1*<sup>-/-</sup> recipients,  
438 and below the detection limit for *Mx1*<sup>+/+</sup> recipients. In order to find an explanation for the seemingly  
439 discrepant data, we examined the liver tissue of bone marrow chimeras at microscopic level 4 days  
440 after THOV infection. Liver tissue from THOV infected *Mx1*<sup>-/-</sup> recipient mice showed lesions. For the  
441 *Mx1*<sup>-/-</sup> mice that received *Mx1*<sup>+/+</sup> bone marrow, the cells in these lesions were in an earlier stage of  
442 cell necrosis compared to *Mx1*<sup>-/-</sup> mice that had been grafted with *Mx1*<sup>-/-</sup> bone marrow cells as cell  
443 nuclei were still visible. The lesions in these mice were also characterized by a clear cellular influx. As

444 a more objective measure for liver damage, the ALT and AST serum levels were determined following  
445 THOV infection. The obtained data reflected the results of the histological analysis of the liver tissue.  
446 This suggests that the expression of a functional Mx1 protein in hematopoietic-derived cells cannot  
447 protect against productive THOV infection in *Mx1*<sup>-/-</sup> recipients, but it can delay disease progression.  
448 This was in line with the THOV infection kinetics data. Histological analysis of liver tissue, as well as  
449 ALT and AST levels in blood serum, showed that *Mx1*<sup>-/-</sup> mice that received *Mx1*<sup>+/+</sup> bone marrow cells  
450 have a delayed progression of liver damage compared with *Mx1*<sup>-/-</sup> mice that received *Mx1*<sup>-/-</sup> bone  
451 marrow cells. Another argument for this theory is that the situation in livers of *Mx1*<sup>-/-</sup> mice that  
452 received *Mx1*<sup>-/-</sup> bone marrow at 2 dpi is comparable with that at 4 dpi in livers of *Mx1*<sup>-/-</sup> mice that  
453 received *Mx1*<sup>+/+</sup> bone marrow. In these two situations we showed comparable liver morbidity and  
454 cellular influx in the liver. Immunohistological analysis made it clear that the cellular influx in the  
455 livers is mainly composed of CD45<sup>+</sup> immune cells. It was apparent that cells that express a functional  
456 Mx1 protein (CD45<sup>+</sup> or CD45<sup>-</sup>) do not express the viral protein NP, which suggests that these cells  
457 were not productively infected. Interestingly, in livers of *Mx1*<sup>-/-</sup> mice that received *Mx1*<sup>-/-</sup> bone  
458 marrow the CD45<sup>+</sup> cells appeared to be the first cells that express the THOV NP.

459

460 Recently, Kochs *et al.* postulated that THOV has a tropism for CD11b<sup>+</sup> cells with a clear  
461 myeloid/macrophage phenotype (double positive for surface markers CD11b and F4/80) in the  
462 peritoneum (54). Therefore, it is conceivable that these cells could be partially protected against  
463 THOV infection by *Mx1* expression. When these cells become infected with THOV, they likely  
464 transport the virus to the liver. This is a credible theory given that Ghosn *et al.* identified a population  
465 of large peritoneal macrophages (LPMs) which seem to have a similar phenotype as the CD11b<sup>+</sup>  
466 myeloid cells described by Kochs *et al.* (54, 55). These LPMs can migrate to the omentum – a fat  
467 tissue that connects the abdominal organs – upon inflammation (56), which is in agreement with the  
468 disappearance of the CD11b<sup>+</sup> myeloid cell population from the peritoneal cavity after THOV infection  
469 (54). From the omentum, the LPMs can reach the liver of infected mice. There, the virus can infect  
470 hepatocytes, unless these hepatocytes express a functional Mx1 protein, in which case, viral  
471 replication would be suppressed in the hepatocytes. In *Mx1*<sup>-/-</sup> mice that received *Mx1*<sup>+/+</sup> bone  
472 marrow we observed high viral titers and necrotic cell lesions in the liver, indicating that THOV can  
473 still reach the liver. However, THOV NP expression in the liver was low to nonexistent. It is plausible  
474 that myeloid cells are only partially protected against THOV infection, or that the viral inoculum  
475 (1000 PFU) used overcomes the Mx1 restriction in the *Mx1*<sup>+/+</sup> myeloid cells. Nonetheless, the  
476 obtained results indicate that *Mx1* expression in myeloid cells can delay the progression of THOV  
477 infection. *Mx1*<sup>+/+</sup> mice that received *Mx1*<sup>-/-</sup> bone marrow showed no detectable liver viral titers and  
478 no liver injury. However, these mice showed clear viral titers in the spleen, which could be explained



479 by the high abundance of myeloid cells in this organ. If THOV could reach the liver tissue via THOV-  
480 susceptible *Mx1*<sup>-/-</sup> myeloid cells, the virus would still be inhibited by the presence of a functional Mx1  
481 protein in the hepatocytes. However, this does not explain the higher weight loss for these mice in  
482 comparison with the *Mx1*<sup>-/-</sup> and *Mx1*<sup>+/+</sup> mice that received *Mx1*<sup>+/+</sup> bone marrow. Conceivably, since  
483 THOV can still reach the liver and spleen quite easily in *Mx1*<sup>+/+</sup> mice that received *Mx1*<sup>-/-</sup> bone  
484 marrow, an inflammatory response will be triggered. This response can cause the production of  
485 inflammatory cytokines (57, 58), and possibly is the reason for the more severe weight loss in *Mx1*<sup>+/+</sup>  
486 mice that received *Mx1*<sup>-/-</sup> bone marrow. Replication in myeloid cells could lead to high type I IFN  
487 levels and lead to a cytokine storm which would explain the severe weight loss in *Mx1*<sup>+/+</sup> mice that  
488 received *Mx1*<sup>-/-</sup> bone marrow (53).

489

490 In conclusion, to confer resistance against Mx1-susceptible viruses that do not have a tropism for  
491 myeloid cells, such as influenza A/Puerto Rico/8/34, *Mx1* expression is primarily important in the  
492 stromal cells. However, for resistance against Mx1-susceptible viruses, like THOV, that can infect  
493 myeloid cells and disseminate through these cells, *Mx1* expression in bone marrow-derived cells is of  
494 major importance.

495 **Acknowledgements**

496 We thank Gnomixx for statistical analysis of the data. We thank Peter Stäheli (University of Freiburg,  
497 Germany) for the helpful discussions and for providing us with the B6.A2G *Mx1<sup>+/+</sup>* mouse strain. We  
498 thank Anne Hoorens (Ghent University Hospital) for expert advice in liver pathology. This study was  
499 supported by IWT-Vlaanderen (Ph.D. student fellowship to JS). The work was funded by the Deutsche  
500 Forschungsgemeinschaft (DFG, German Research Foundation) - KO 1579/12-1 to GK.

501

502 **References**

- 503 1. **Verhelst J, Hulpiau P, Saelens X.** 2013. Mx proteins: antiviral gatekeepers that restrain the  
504 uninvited. *Microbiology and molecular biology reviews* : MMBR **77**:551-566.
- 505 2. **Horisberger MA, Staeheli P, Haller O.** 1983. Interferon induces a unique protein in mouse  
506 cells bearing a gene for resistance to influenza virus. *Proceedings of the National Academy of*  
507 *Sciences of the United States of America* **80**:1910-1914.
- 508 3. **Staeheli P, Haller O.** 1985. Interferon-induced human protein with homology to protein Mx  
509 of influenza virus-resistant mice. *Molecular and cellular biology* **5**:2150-2153.
- 510 4. **Holzinger D, Jorns C, Stertz S, Boisson-Dupuis S, Thimme R, Weidmann M, Casanova JL,**  
511 **Haller O, Kochs G.** 2007. Induction of MxA gene expression by influenza A virus requires type  
512 I or type III interferon signaling. *Journal of virology* **81**:7776-7785.
- 513 5. **Pavlovic J, Haller O, Staeheli P.** 1992. Human and mouse Mx proteins inhibit different steps  
514 of the influenza virus multiplication cycle. *Journal of virology* **66**:2564-2569.
- 515 6. **Verhelst J, Parthoens E, Schepens B, Fiers W, Saelens X.** 2012. Interferon-inducible protein  
516 Mx1 inhibits influenza virus by interfering with functional viral ribonucleoprotein complex  
517 assembly. *Journal of virology* **86**:13445-13455.
- 518 7. **Nigg PE, Pavlovic J.** 2015. Oligomerization and GTP-binding Requirements of MxA for Viral  
519 Target Recognition and Antiviral Activity against Influenza A Virus. *The Journal of biological*  
520 *chemistry* **290**:29893-29906.
- 521 8. **Zimmermann P, Manz B, Haller O, Schwemmle M, Kochs G.** 2011. The viral nucleoprotein  
522 determines Mx sensitivity of influenza A viruses. *Journal of virology* **85**:8133-8140.
- 523 9. **Manz B, Dornfeld D, Gotz V, Zell R, Zimmermann P, Haller O, Kochs G, Schwemmle M.** 2013.  
524 Pandemic influenza A viruses escape from restriction by human MxA through adaptive  
525 mutations in the nucleoprotein. *PLoS pathogens* **9**:e1003279.
- 526 10. **Carr JF, Hinshaw JE.** 1997. Dynamin assembles into spirals under physiological salt conditions  
527 upon the addition of GDP and gamma-phosphate analogues. *The Journal of biological*  
528 *chemistry* **272**:28030-28035.
- 529 11. **Daumke O, Gao S, von der Malsburg A, Haller O, Kochs G.** 2010. Structure of the MxA stalk  
530 elucidates the assembly of ring-like units of an antiviral module. *Small GTPases* **1**:62-64.
- 531 12. **Gao S, von der Malsburg A, Paeschke S, Behlke J, Haller O, Kochs G, Daumke O.** 2010.  
532 Structural basis of oligomerization in the stalk region of dynamin-like MxA. *Nature* **465**:502-  
533 506.
- 534 13. **Hinshaw JE, Schmid SL.** 1995. Dynamin self-assembles into rings suggesting a mechanism for  
535 coated vesicle budding. *Nature* **374**:190-192.
- 536 14. **Kochs G, Haener M, Aebi U, Haller O.** 2002. Self-assembly of human MxA GTPase into highly  
537 ordered dynamin-like oligomers. *The Journal of biological chemistry* **277**:14172-14176.
- 538 15. **Verhelst J, Van Hoecke L, Spitaels J, De Vlioger D, Kolpe A, Saelens X.** 2017. Chemical-  
539 controlled Activation of Antiviral Myxovirus Resistance Protein 1. *The Journal of biological*  
540 *chemistry* **292**:2226-2236.

- 541 16. **Chen Y, Zhang L, Graf L, Yu B, Liu Y, Kochs G, Zhao Y, Gao S.** 2017. Conformational dynamics  
542 of dynamin-like MxA revealed by single-molecule FRET. *Nature communications* **8**:15744.
- 543 17. **Haller O, Frese M, Rost D, Nuttall PA, Kochs G.** 1995. Tick-borne thogoto virus infection in  
544 mice is inhibited by the orthomyxovirus resistance gene product Mx1. *Journal of virology*  
545 **69**:2596-2601.
- 546 18. **Kochs G, Haller O.** 1999. GTP-bound human MxA protein interacts with the nucleocapsids of  
547 Thogoto virus (Orthomyxoviridae). *The Journal of biological chemistry* **274**:4370-4376.
- 548 19. **Kochs G, Haller O.** 1999. Interferon-induced human MxA GTPase blocks nuclear import of  
549 Thogoto virus nucleocapsids. *Proceedings of the National Academy of Sciences of the United*  
550 *States of America* **96**:2082-2086.
- 551 20. **Hause BM, Ducatez M, Collin EA, Ran Z, Liu R, Sheng Z, Armien A, Kaplan B, Chakravarty S,**  
552 **Hoppe AD, Webby RJ, Simonson RR, Li F.** 2013. Isolation of a novel swine influenza virus  
553 from Oklahoma in 2011 which is distantly related to human influenza C viruses. *PLoS*  
554 *pathogens* **9**:e1003176.
- 555 21. **McCauley JW, Hongo S, Kaverin NV, Kochs G, Lamb RA, Matrosovich MN.** 2012. Family  
556 Orthomyxoviridae, p. 749-761. *In* King AM, Adams MJ, Carstens EB, Lefkowitz EJ (ed.), *Virus*  
557 *taxonomy: classification and nomenclature of viruses. Ninth report of the International*  
558 *Committee of Taxonomy of Viruses.* Elsevier, New York.
- 559 22. **Presti RM, Zhao G, Beatty WL, Mihindikulasuriya KA, da Rosa AP, Popov VL, Tesh RB,**  
560 **Virgin HW, Wang D.** 2009. Quarantfil, Johnston Atoll, and Lake Chad viruses are novel  
561 members of the family Orthomyxoviridae. *Journal of virology* **83**:11599-11606.
- 562 23. **Moore DL, Causey OR, Carey DE, Reddy S, Cooke AR, Akinkugbe FM, David-West TS, Kemp**  
563 **GE.** 1975. Arthropod-borne viral infections of man in Nigeria, 1964-1970. *Annals of tropical*  
564 *medicine and parasitology* **69**:49-64.
- 565 24. **Darwish MA, Hoogstraal H, Omar FM.** 1979. A serological survey for Thogoto virus in  
566 humans, domestic mammals, and rats in Egypt. *The Journal of the Egyptian Public Health*  
567 *Association* **54**:1-8.
- 568 25. **Te Velthuis AJ, Fodor E.** 2016. Influenza virus RNA polymerase: insights into the mechanisms  
569 of viral RNA synthesis. *Nature reviews. Microbiology* **14**:479-493.
- 570 26. **Lakdawala SS, Fodor E, Subbarao K.** 2016. Moving On Out: Transport and Packaging of  
571 Influenza Viral RNA into Virions. *Annual review of virology* **3**:411-427.
- 572 27. **Fuller FJ, Freedman-Faulstich EZ, Barnes JA.** 1987. Complete nucleotide sequence of the tick-  
573 borne, orthomyxo-like Dhori/Indian/1313/61 virus nucleoprotein gene. *Virology* **160**:81-87.
- 574 28. **Kochs G, Weber F, Gruber S, Delvendahl A, Leitz C, Haller O.** 2000. Thogoto virus matrix  
575 protein is encoded by a spliced mRNA. *Journal of virology* **74**:10785-10789.
- 576 29. **Leahy MB, Dessens JT, Weber F, Kochs G, Nuttall PA.** 1997. The fourth genus in the  
577 Orthomyxoviridae: sequence analyses of two Thogoto virus polymerase proteins and  
578 comparison with influenza viruses. *Virus research* **50**:215-224.
- 579 30. **Weber F, Gruber S, Haller O, Kochs G.** 1999. PB2 polymerase subunit of Thogoto virus  
580 (Orthomyxoviridae family). *Archives of virology* **144**:1601-1609.
- 581 31. **Weber F, Haller O, Kochs G.** 1996. Nucleoprotein viral RNA and mRNA of Thogoto virus: a  
582 novel "cap-stealing" mechanism in tick-borne orthomyxoviruses? *Journal of virology*  
583 **70**:8361-8367.
- 584 32. **Hagmaier K, Jennings S, Buse J, Weber F, Kochs G.** 2003. Novel gene product of Thogoto  
585 virus segment 6 codes for an interferon antagonist. *Journal of virology* **77**:2747-2752.
- 586 33. **Vogt C, Preuss E, Mayer D, Weber F, Schwemmler M, Kochs G.** 2008. The interferon  
587 antagonist ML protein of thogoto virus targets general transcription factor IIB. *Journal of*  
588 *virology* **82**:11446-11453.
- 589 34. **Portela A, Jones LD, Nuttall P.** 1992. Identification of viral structural polypeptides of Thogoto  
590 virus (a tick-borne orthomyxo-like virus) and functions associated with the glycoprotein. *The*  
591 *Journal of general virology* **73 ( Pt 11)**:2823-2830.

- 592 35. **Yang M, Feng F, Liu Y, Wang H, Yang Z, Hou W, Liang H.** 2016. pH-dependent conformational  
593 changes of a Thogoto virus matrix protein reveal mechanisms of viral assembly and  
594 uncoating. *The Journal of general virology* **97**:2149-2156.
- 595 36. **Siebler J, Haller O, Kochs G.** 1996. Thogoto and Dhori virus replication is blocked by  
596 inhibitors of cellular polymerase II activity but does not cause shutoff of host cell protein  
597 synthesis. *Archives of virology* **141**:1587-1594.
- 598 37. **Weber F, Jambrina E, Gonzalez S, Dessens JT, Leahy M, Kochs G, Portela A, Nuttall PA,**  
599 **Haller O, Ortin J, Zurcher T.** 1998. In vivo reconstitution of active Thogoto virus polymerase:  
600 assays for the compatibility with other orthomyxovirus core proteins and template RNAs.  
601 *Virus research* **58**:13-20.
- 602 38. **Albo C, Martin J, Portela A.** 1996. The 5' ends of Thogoto virus (Orthomyxoviridae) mRNAs  
603 are homogeneous in both length and sequence. *Journal of virology* **70**:9013-9017.
- 604 39. **Guilligay D, Kadlec J, Crepin T, Lunardi T, Bouvier D, Kochs G, Ruigrok RW, Cusack S.** 2014.  
605 Comparative structural and functional analysis of orthomyxovirus polymerase cap-snatching  
606 domains. *PLoS one* **9**:e84973.
- 607 40. **Wagner E, Engelhardt OG, Weber F, Haller O, Kochs G.** 2000. Formation of virus-like  
608 particles from cloned cDNAs of Thogoto virus. *The Journal of general virology* **81**:2849-2853.
- 609 41. **Pulverer JE, Rand U, Lienenklaus S, Kugel D, Zietara N, Kochs G, Naumann R, Weiss S,**  
610 **Staehele P, Hauser H, Koster M.** 2010. Temporal and spatial resolution of type I and III  
611 interferon responses in vivo. *Journal of virology* **84**:8626-8638.
- 612 42. **Mateo RI, Xiao SY, Lei H, AP DAR, Tesh RB.** 2007. Dhori virus (Orthomyxoviridae:  
613 Thogotovirus) infection in mice: a model of the pathogenesis of severe orthomyxovirus  
614 infection. *The American journal of tropical medicine and hygiene* **76**:785-790.
- 615 43. **Haller O, Lindenmann J.** 1974. Athymic (nude) mice express gene for myxovirus resistance.  
616 *Nature* **250**:679-680.
- 617 44. **Haller O, Arnheiter H, Lindenmann J.** 1979. Natural, genetically determined resistance  
618 toward influenza virus in hemopoietic mouse chimeras. Role of mononuclear phagocytes.  
619 *The Journal of experimental medicine* **150**:117-126.
- 620 45. **Staehele P, Grob R, Meier E, Sutcliffe JG, Haller O.** 1988. Influenza virus-susceptible mice  
621 carry Mx genes with a large deletion or a nonsense mutation. *Molecular and cellular biology*  
622 **8**:4518-4523.
- 623 46. **Cho KJ, Schepens B, Seok JH, Kim S, Roose K, Lee JH, Gallardo R, Van Hamme E,**  
624 **Schymkowitz J, Rousseau F, Fiers W, Saelens X, Kim KH.** 2015. Structure of the extracellular  
625 domain of matrix protein 2 of influenza A virus in complex with a protective monoclonal  
626 antibody. *Journal of virology* **89**:3700-3711.
- 627 47. **Baird D, Murray D, Payne R, Soutar D.** 2017. An Introduction to GenStat for Windows (19th  
628 Edition), GenStat, vol. 19.
- 629 48. **Wakim LM, Gupta N, Minter JD, Villadangos JA.** 2013. Enhanced survival of lung tissue-  
630 resident memory CD8(+) T cells during infection with influenza virus due to selective  
631 expression of IFITM3. *Nature immunology* **14**:238-245.
- 632 49. **Helft J, Manicassamy B, Guernonprez P, Hashimoto D, Silvin A, Agudo J, Brown BD,**  
633 **Schmolke M, Miller JC, Leboeuf M, Murphy KM, Garcia-Sastre A, Merad M.** 2012. Cross-  
634 presenting CD103+ dendritic cells are protected from influenza virus infection. *The Journal of*  
635 *clinical investigation* **122**:4037-4047.
- 636 50. **Molledo B, Li W, Yount JS, Moran TM.** 2011. Unique type I interferon responses determine  
637 the functional fate of migratory lung dendritic cells during influenza virus infection. *PLoS*  
638 *pathogens* **7**:e1002345.
- 639 51. **Merad M, Manz MG, Karsunky H, Wagers A, Peters W, Charo I, Weissman IL, Cyster JG,**  
640 **Engleman EG.** 2002. Langerhans cells renew in the skin throughout life under steady-state  
641 conditions. *Nature immunology* **3**:1135-1141.
- 642 52. **Sugrue T, Lowndes NF, Ceredig R.** 2013. Mesenchymal stromal cells: radio-resistant  
643 members of the bone marrow. *Immunology and cell biology* **91**:5-11.

- 644 53. **Li H, Bradley KC, Long JS, Frise R, Ashcroft JW, Hartgroves LC, Shelton H, Makris S,**  
645 **Johansson C, Cao B, Barclay WS.** 2018. Internal genes of a highly pathogenic H5N1 influenza  
646 virus determine high viral replication in myeloid cells and severe outcome of infection in  
647 mice. *PLoS pathogens* **14**:e1006821.
- 648 54. **Kochs G, Anzaghe M, Kronhart S, Wagner V, Gogesch P, Scheu S, Lienenklaus S, Waibler Z.**  
649 **2016. In Vivo Conditions Enable IFNAR-Independent Type I Interferon Production by**  
650 **Peritoneal CD11b+ Cells upon Thogoto Virus Infection. *Journal of virology* **90**:9330-9337.**
- 651 55. **Ghosh EE, Cassado AA, Govoni GR, Fukuhara T, Yang Y, Monack DM, Bortoluci KR, Almeida**  
652 **SR, Herzenberg LA, Herzenberg LA.** 2010. Two physically, functionally, and developmentally  
653 distinct peritoneal macrophage subsets. *Proceedings of the National Academy of Sciences of*  
654 *the United States of America* **107**:2568-2573.
- 655 56. **Okabe Y, Medzhitov R.** 2014. Tissue-specific signals control reversible program of localization  
656 and functional polarization of macrophages. *Cell* **157**:832-844.
- 657 57. **Racanelli V, Rehermann B.** 2006. The liver as an immunological organ. *Hepatology* **43**:S54-  
658 62.
- 659 58. **Tilg H.** 2001. Cytokines and liver diseases. *Canadian journal of gastroenterology = Journal*  
660 *canadien de gastroenterologie* **15**:661-668.

661

662 **Figure legends**

663

664 **Figure 1**

665

666 **Mx1-mediated resistance to influenza A virus infection primarily depends on the genotype of the**  
667 **recipient bone marrow chimeric mice. (A)** Schematic overview of the generation of the bone  
668 marrow chimeras. The PCR-based genotyping of the donor and acceptor mice is also depicted. **(B)**  
669 Mice (n = 14 per group) were infected intranasally with 10 LD<sub>50</sub> of maPR8 virus and the body weight  
670 change over time after infection was monitored. Data points represent the average of 14 mice from 0  
671 dpi until 3 dpi, and the average of 7 mice from 4 dpi until 6 dpi. Error bars represent the standard  
672 error of the mean. Asterisks indicate the significant difference between the *Mx1*<sup>-/-</sup> → *Mx1*<sup>-/-</sup> group  
673 and all other groups over time. \*\*\*, p < 0.001. Circles indicate the significant difference with the  
674 *Mx1*<sup>+/+</sup> → *Mx1*<sup>-/-</sup> group over time. °, p < 0.01; °°, p < 0.001. **(C)** Mice were sacrificed on 3 and 6 days  
675 post infection and lung viral loads were determined. Each data point represents the lung viral titer of  
676 a single animal. Asterisks indicate the significant difference between the *Mx1*<sup>-/-</sup> → *Mx1*<sup>-/-</sup> group and  
677 all other groups. \*\*, p < 0.01; \*\*\*, p < 0.001. Circles indicate the significant difference between the  
678 *Mx1*<sup>+/+</sup> → *Mx1*<sup>-/-</sup> group and all other groups. °, p < 0,05; °°, p < 0,01; °°,°°, p < 0.0001. **(D)** Viral mRNA  
679 load in lung homogenates from mice sacrificed on day 3 and 6 after infection as determined by RT-  
680 qPCR. Data points represent the average levels of total viral mRNA relative to household genes. Error  
681 bars represent standard error of the mean. Asterisks indicate the significant difference between the  
682 *Mx1*<sup>-/-</sup> → *Mx1*<sup>-/-</sup> group and all other groups. \*\*\*, p < 0.001. Circles indicate the significant difference  
683 between the *Mx1*<sup>+/+</sup> → *Mx1*<sup>-/-</sup> group and all other groups. °°, p < 0.001. **(E)** Viral mRNA load of the  
684 eight separate influenza virus genome segments in lung homogenates from the respective bone  
685 marrow chimeric mice sacrificed on day 6 after infection as determined by RT-qPCR. Bars represent  
686 the average levels of viral mRNA relative to household genes. Error bars represent standard error of  
687 the mean. The data are pooled from 2 independently performed experiments (first experiment n = 6  
688 and second experiment n = 8).

689 **Figure 2**

690

691 ***Mx1*<sup>+/+</sup> hematopoietic cells contribute to protection against THOV-associated pathology.** Bone  
692 marrow chimeric mice were infected intraperitoneally with 1000 PFU of THOV on day 0. **(A)** Body  
693 weight change over time after infection. Data points represent the average of eight mice. Error bars  
694 represent the standard error of the mean. Statistical analysis was done using a two-way ANOVA with  
695 post hoc Tukey's HSD test. Asterisks indicate the significant difference between the *Mx1*<sup>-/-</sup> → *Mx1*<sup>-/-</sup>

696 group and all other groups. \*,  $p < 0.05$ ; \*\*,  $p < 0.01$ ; \*\*\*\*,  $p < 0.0001$ . Circles indicate the significant  
697 difference between the  $Mx1^{+/+} \rightarrow Mx1^{-/-}$  group and all other groups. °,  $p < 0.01$ ; °°,  $p < 0.001$ ; °°,°°,  $p$   
698  $< 0.0001$ . Caps indicate the significant difference between the  $Mx1^{-/-} \rightarrow Mx1^{+/+}$  group and all other  
699 groups. ^,  $p < 0.05$ ; ^^,  $p < 0.0001$ . **(B)** Viral titers determined by plaque assay in the liver on day 4  
700 after infection. Each data point represents the liver viral titer of a single animal. Statistical analysis  
701 was performed using Kruskal-Wallis test with post hoc Dunn's multiple comparison test. Asterisks  
702 indicate the significant difference between the  $Mx1^{-/-} \rightarrow Mx1^{-/-}$  group and all other groups. \*\*\*,  $p <$   
703  $0.001$ . Circles indicate the significant difference between the  $Mx1^{+/+} \rightarrow Mx1^{-/-}$  group and all other  
704 groups. °,  $p < 0.05$ . Data are pooled from 2 independently performed experiments (first experiment  $n$   
705  $= 4$ , second experiment  $n = 4$ ). **(C)** Histological analysis of liver tissue section (5  $\mu\text{m}$  slides) after 4 days  
706 of infection stained with hematoxylin and eosin. Arrows indicate focal zones of liver cell necrosis.  
707 Scale bar = 100  $\mu\text{m}$ . Pictures are representative for  $n = 8$ . Serum concentrations of ALT **(D)** and AST  
708 **(E)** determined on day 4 after infection. Each data point represents the ALT or AST concentration of a  
709 single animal ( $n = 4$ ). Asterisks indicate the significant difference between the  $Mx1^{-/-} \rightarrow Mx1^{-/-}$  group  
710 and all other groups. \*,  $p < 0.05$ ; \*\*,  $p < 0.01$ ; Kruskal-Wallis test with post hoc Dunn's multiple  
711 comparison test.

712

### 713 **Figure 3**

714

715  **$Mx1^{+/+}$  immune cells delay THOV-associated liver damage in B6.A2G  $Mx1^{-/-}$  recipient mice.**  
716 Radiation chimeric mice ( $n = 19$  per group) were generated and infected intraperitoneally with 1000  
717 PFU of THOV. Before infection ( $n = 5$ ), and on day 2 ( $n = 6$ ) and 4 ( $n = 8$ ) after infection, mice were  
718 sacrificed and liver and serum samples were prepared. **(A)** Representative photo micrographs of liver  
719 section stained with hematoxylin and eosin. Arrows indicate focal zones of liver cell necrosis. Scale  
720 bar = 100  $\mu\text{m}$ . Serum concentrations of ALT **(B)** and AST **(C)**. Each data point represents the ALT or  
721 AST concentration of a single animal. Asterisks indicate the significant difference between the  $Mx1^{-/-}$   
722  $\rightarrow Mx1^{-/-}$  group and all other groups. \*\*\*\*,  $p < 0.0001$ . Data are pooled from 2 independently  
723 performed experiments (first experiment  $n = 9$ , second experiment  $n = 10$ ).

724

### 725 **Figure 4**

726

727  **$Mx1$  in hematopoietic cells differentially controls THOV replication in different parts of the body.**  
728 Bone marrow chimeric mice ( $n = 14$  per group) were generated and infected intraperitoneally with  
729 1000 PFU of THOV. On day 2 ( $n = 6$ ) and 4 ( $n = 8$ ) after infection, mice were sacrificed and viral titers  
730 in liver **(A)**, lung **(B)**, spleen **(C)**, and serum **(D)** were determined. Each data point represents the viral

731 titer of a single animal. Asterisks indicate the significant difference between the  $Mx1^{-/-} \rightarrow Mx1^{-/-}$   
732 group and all other groups. \*\*,  $p < 0,01$ ; \*\*\*,  $p < 0.001$ ; \*\*\*\*,  $p < 0,0001$ . Circles indicate the  
733 significant difference between the  $Mx1^{+/+} \rightarrow Mx1^{-/-}$  group and all other groups. °,  $p < 0.05$ . Caps  
734 indicate the significant difference between the  $Mx1^{-/-} \rightarrow Mx1^{+/+}$  group and all other groups. ^,  $p <$   
735  $0.05$ . Data are pooled from 2 independently performed experiments (first experiment  $n = 7$ , second  
736 experiment  $n = 7$ ).

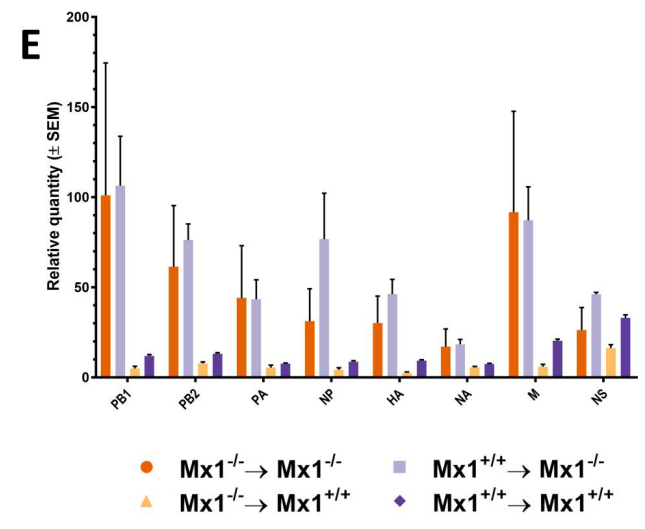
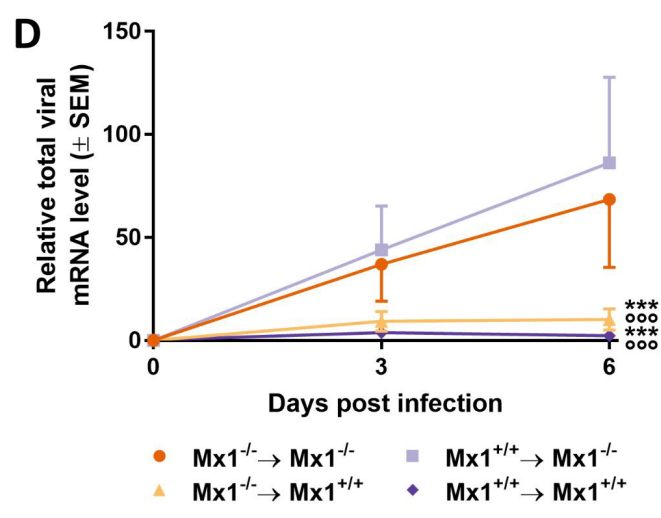
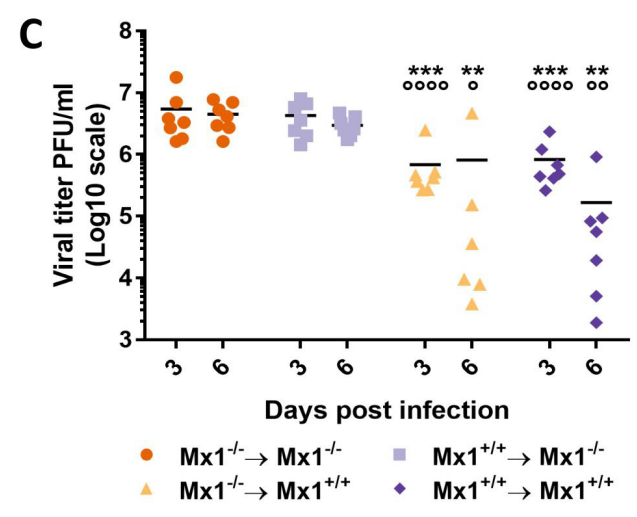
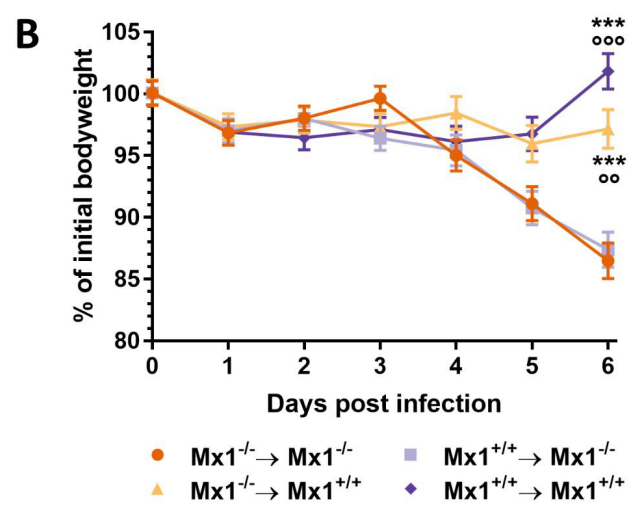
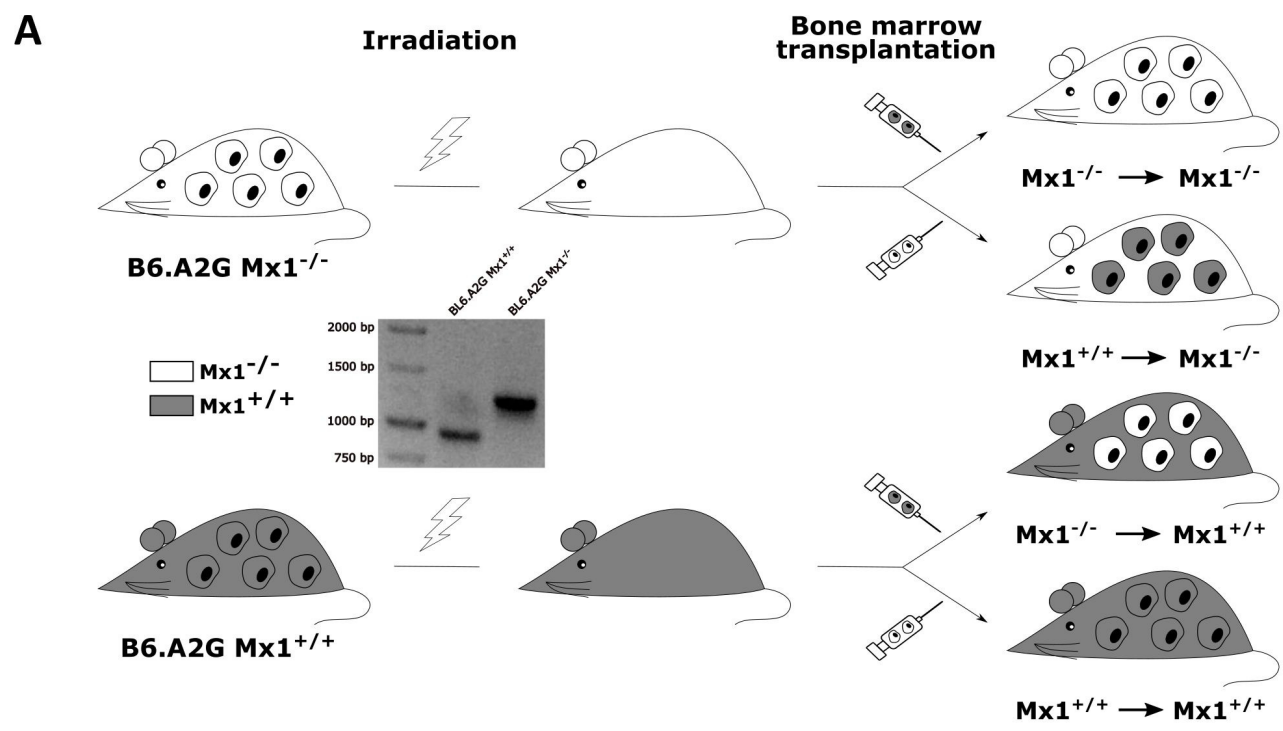
737

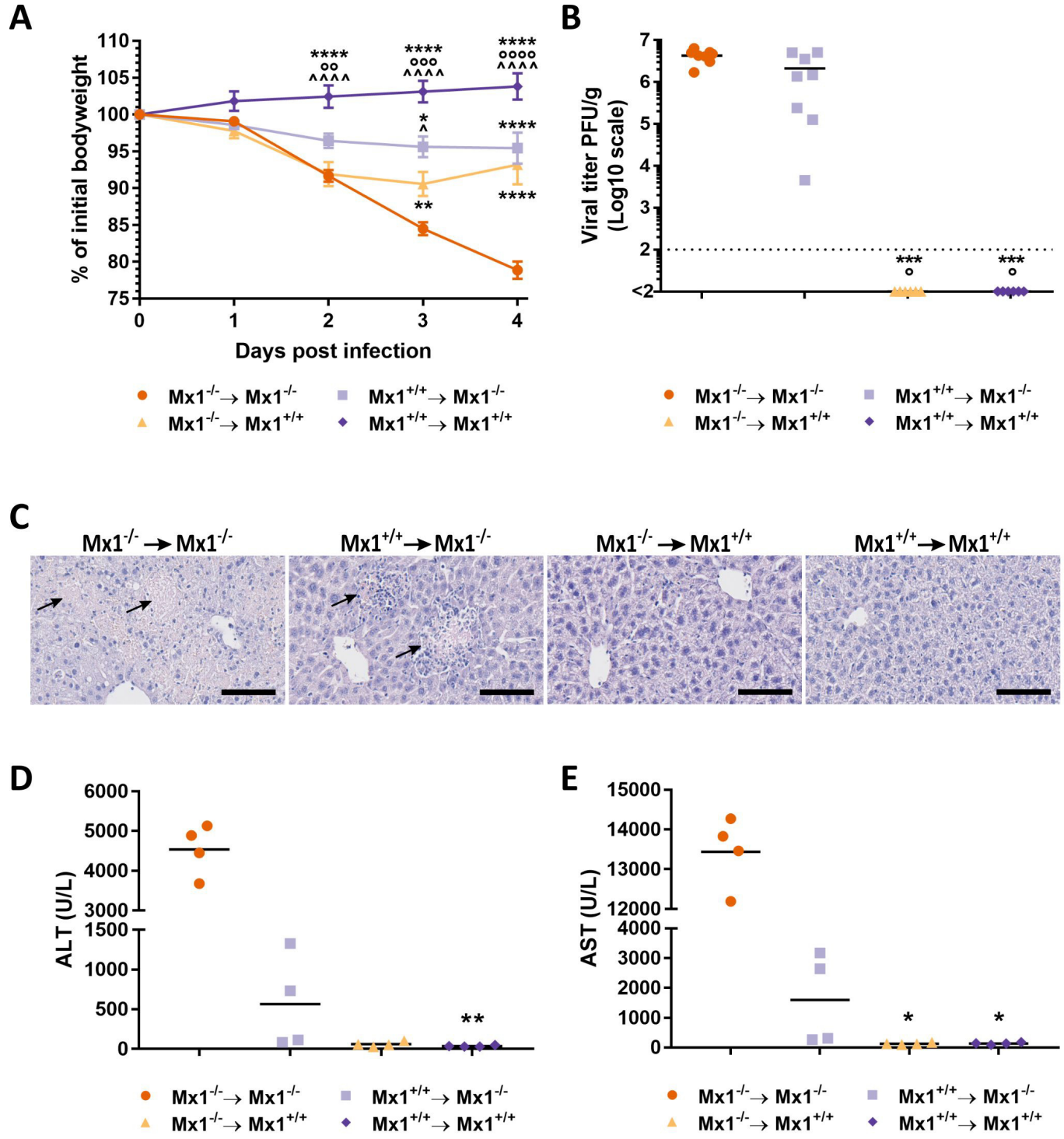
738 **Figure 5**

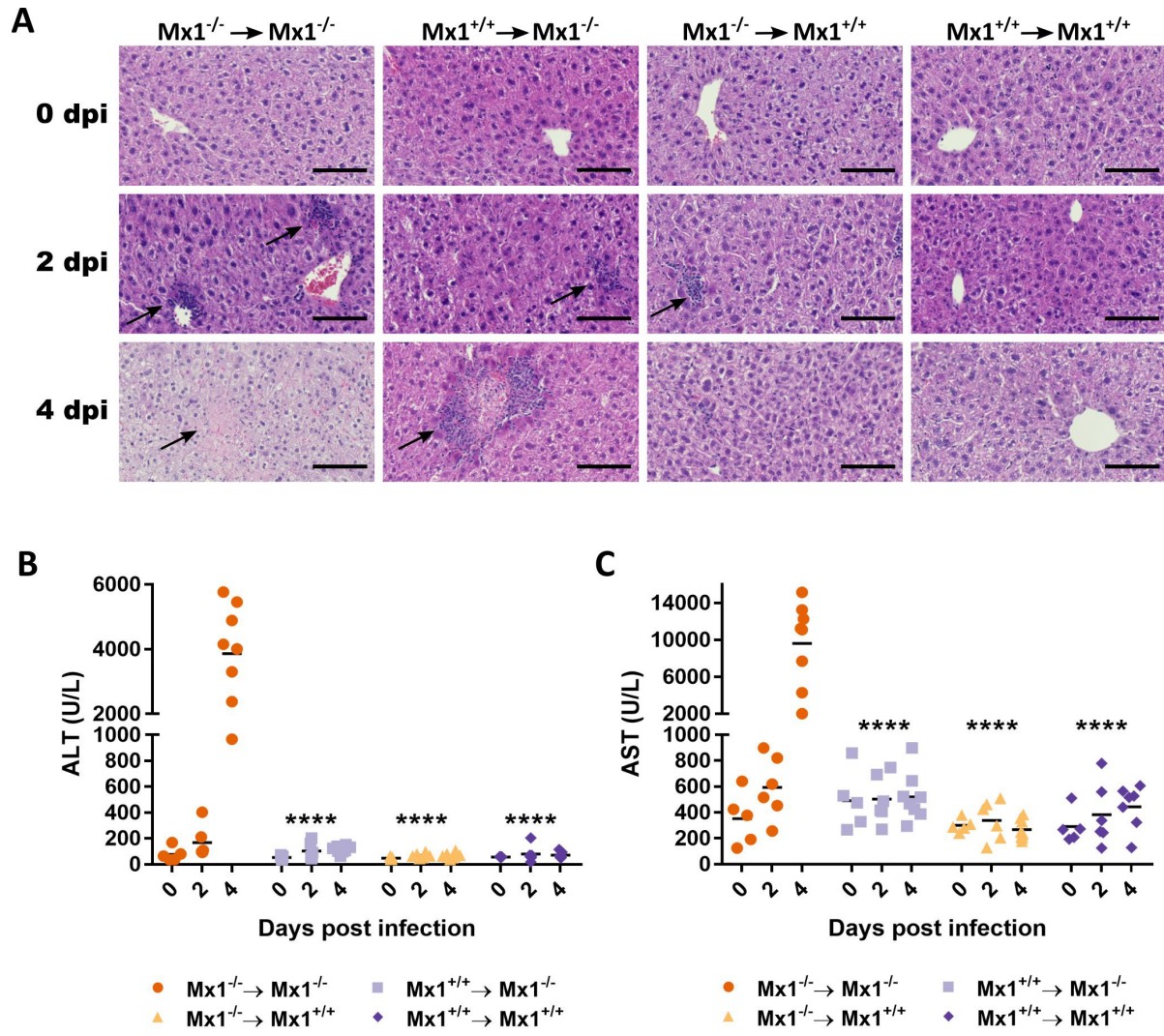
739

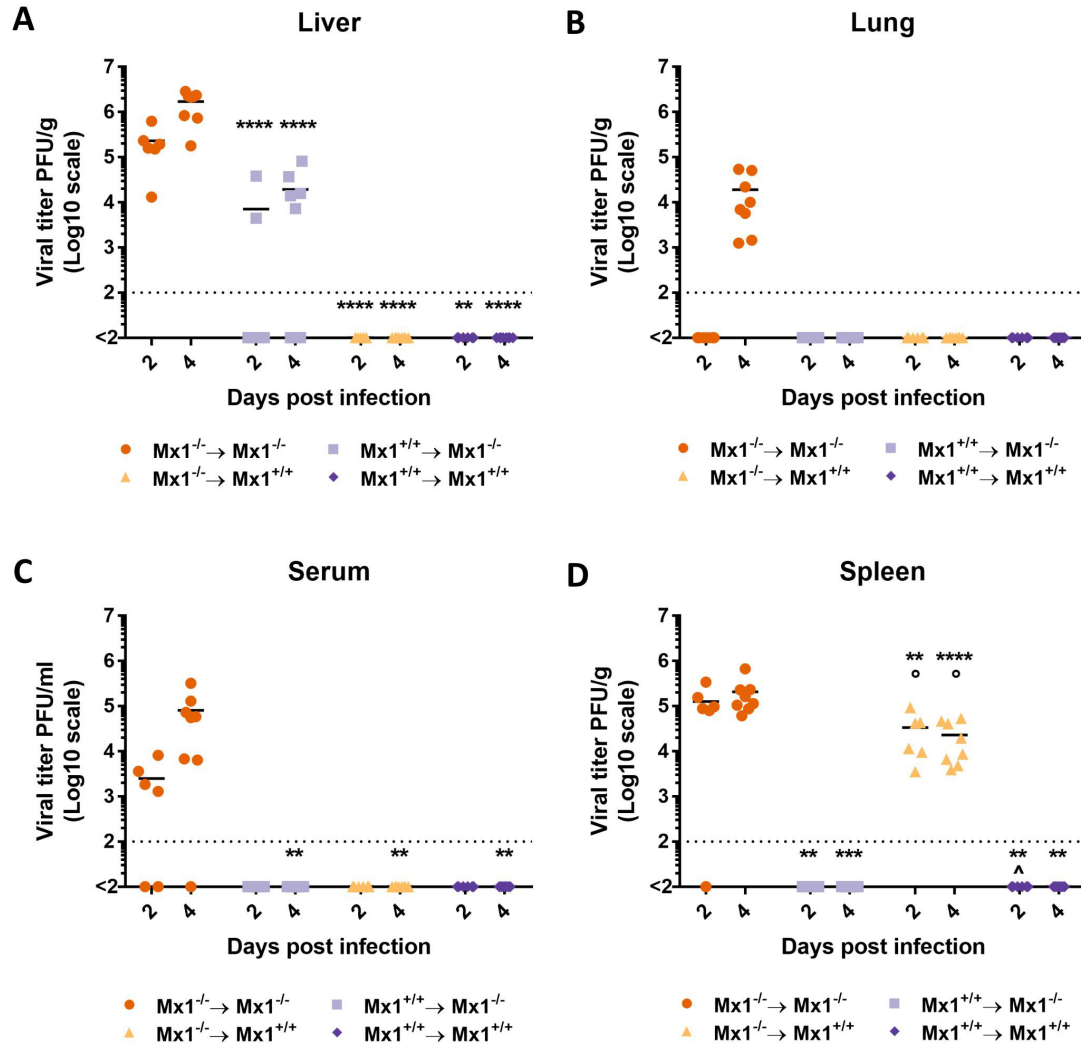
740  **$Mx1^{+/+}$  hematopoietic cells delay THOV infection-associated liver damage in B6.A2G  $Mx1^{-/-}$**   
741 **recipient mice.** Bone marrow chimeric mice ( $n = 19$  per group) were infected intraperitoneally with  
742 1000 PFU of THOV. Before infection (0 dpi) ( $n = 5$ ), 2 ( $n = 6$ ) and 4 ( $n = 8$ ) days after infection mice  
743 were sacrificed, livers were isolated, and prepared for histological analysis by staining tissue slides  
744 with hematoxylin and immunostaining with polyclonal antiserum directed against THOV NP and Mx1,  
745 or a monoclonal antibody against CD45. Scale bar = 100  $\mu\text{m}$ .

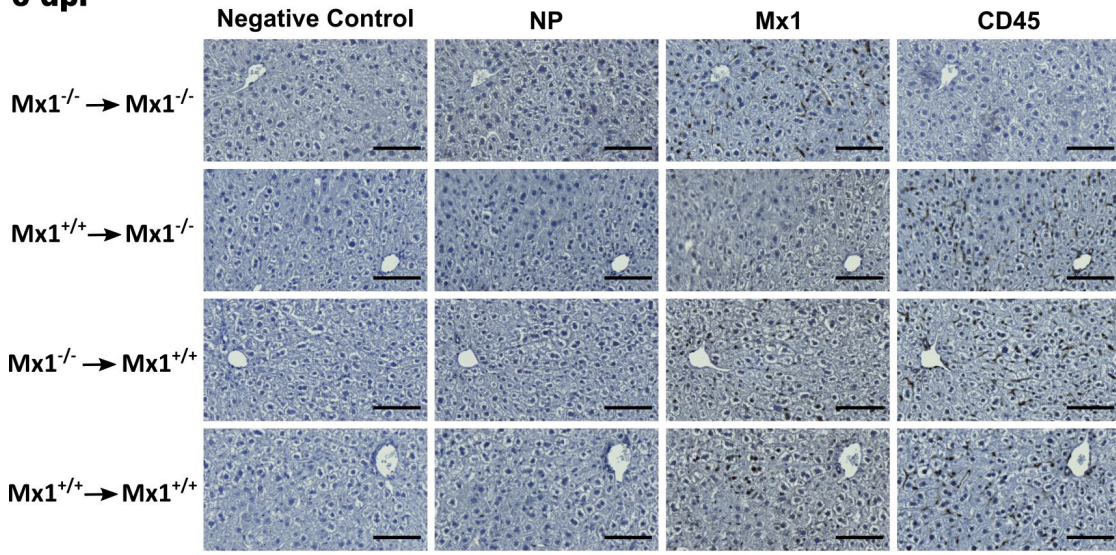
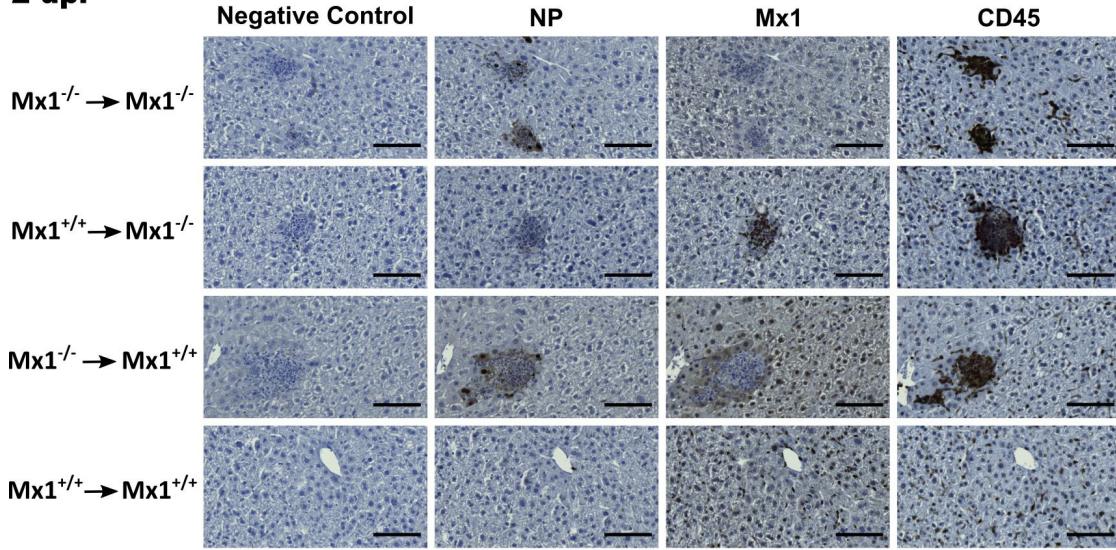










**0 dpi****2 dpi****4 dpi**